Available online at www.sciencedirect.com

ScienceDirect

Procedia Structural Integrity 8 (2018) 604–609

Structural Integrity Procedia

www.elsevier.com/locate/procedia

AIAS 2017 International Conference on Stress Analysis, AIAS 2017, 6–9 September 2017, Pisa, Italy

Analysis of debonding in bio-inspired interfaces obtained by additive manufacturing

Marco Alfano*, Chiara Morano, Luigi Bruno, Maurizio Muzzupappa, Leonardo Pagnotta

Department of Mechanical, Energy and Management Engineering, University of Calabria, P. Bucci 44C, Italy

Abstract

The present work is focused on the analysis of fracture in adhesive bonded Double Cantilever Beam (DCB) specimens with 3D printed nylon substrates. The substrates were obtained using selective laser sintering of polyamide powder and embed sub-surface channels with circular and square cross-section. The proposed strategy allows to mimic the crack trapping effect already observed in a multitude of biological materials, that is originated by the spatial modulation of the driving force available for crack growth. Mechanical tests have shown that the channels induce load fluctuations in the global load-displacement response. A significant increase in the total dissipated energy was observed with respect to bulk samples, *i.e.* no channels. The observed fluctuations in the global response were associated to the sequential storage and sudden release of elastic energy. Indeed, the spatial modulation of the stiffness around the interfacial region ultimately affects the crack driving force.

Peer-review under responsibility of the Scientific Committee of AIAS 2017 International Conference on Stress Analysis

Keywords: selective laser sintering, bio-inspired interfaces, double cantilever beam, crack trapping

1. Introduction

Several works in the broad area of biological materials indicated that the surface and sub-surface features of bush crickets or geckos are provided with extraordinary adhesion properties, see for instance Jagota and Hui (2011). It has been shown that subsurface structures, such as those observed in the barnacles by Hui et al. (2015), enable the so called *crack trapping* effect. Previous works, such as that of Beese et al. (2014), indicated that crack trapping is commonly observed in biological materials which feature a periodic distribution of phases with distinct stiffness within the material architecture. Majumder et al. (2010), Afferrante and Carbone (2011) and Afferrante et al. (2015) highlighted that crack trapping is due to the modulation of the driving force which arises because of the above mentioned stiffness variation. The effect has been reproduced experimentally by resorting to standard micro-lithography techniques Glassmaker et al. (2007). More recently, thanks to the ability to fabricate complex geometries, additive manufacturing

* Corresponding author. Tel.: +39-0984-494156 ; fax: +39-0984-494673.
E-mail address: marco.alfano@unical.it

Peer-review under responsibility of the Scientific Committee of AIAS 2017 International Conference on Stress Analysis
10.1016/j.prostr.2017.12.059

has emerged as a very effective approach for prototyping mechanical components and is a powerful platform for the experimental study of bio-inspired materials, *e.g*. Lin et al. (2014), Libonati et al. (2016). The present work is focused on the analysis of fracture in adhesive bonded Double Cantilever Beam (DCB) specimens with 3D printed bio-inspired interfaces. The substrates, obtained using Selective Laser Sintering (SLS) of polyamide powder, embed sub-surface channels with either circular or square cross-sections. Adhesive bonding has been carried out using a structural epoxy adhesive. Surface pre-treatments consisted of ultrasonic cleaning in acetone and oven drying. Mechanical testing was carried out using an electromechanical testing machine. High resolution imaging is finally deployed to unravel the mechanisms of failure.

2. Materials and methods

2.1. Sample fabrication

Sample fabrication has been carried out using selective laser sintering (Formiga P110, EOS, Germania) of poliammide powders (EOSINT P/PA2200). Dogbone samples were initially prepared to assess the bulk material properties. The procedures and recommendations reported in the ASTM D638-14 were followed. Moreover, fracture tests were also carried out using peel loaded adhesive bonded Double Cantilever Beam (DCB) configuration. The substrates length and width were equal to 150 mm and 15 mm, respectively. Three sets of substrates have been prepared: (i) bulk substrates with no pattern as well as patterned substrates with (ii) circular and (iii) square subsurface channels. The precise dimensions of the channels have been selected with the support of finite element simulations carried out using an in-house developed finite element software. The samples were coupled to the testing machine through loading blocks, which were included in the 3D CAD model employed for SLS. A schematic of the dogbone sample and DCB arms is provided in Fig. 1 along with the corresponding dimensions. The DCB arms were subsequently bonded using a bi-component structural epoxy adhesive (Hysol 9466, Henkel, Germany). Surface preparation prior to bonding included ultrasonic cleaning in acetone bath for 5 minutes followed by oven cooling at 30°C for 2 minutes. Nylon wires were used as spacers to set an adhesive bondline thickness equal to 0.2 mm. A uniform pressure was exerted using weights so that to squeeze out the adhesive in excess. Adhesive curing was performed at room temperature.

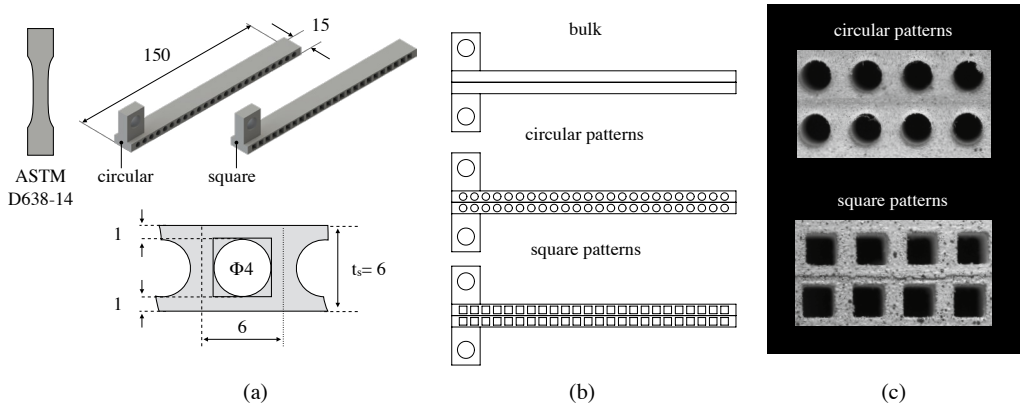

Fig. 1: (a) 3D printed nylon dogbone sample and DCB arms featuring subsurface channels with square and circular shape. The relevant geometrical dimensions of the subsurface channels are also shown. (b) Schematic representation of the bonded DCB samples analyzed in this work. (c) Snapshot of the actual 3D printed DCB samples taken during mechanical tests.

2.2. Mechanical tests

Mechanical tests were carried out using an electromechanical testing machine (MTS Criterion, Model 42) provided with a 5 kN load cell. Tensile tests were performed using a cross-head displacement rate equal to 0.5 mm/min. In order to determine the Poisson ratio, Digital Image Correlation (DIC) was used to resolve the displacement field in a region

of interest (ROI) within the gauge length of the samples. The surface of the specimen was covered with a random speckle pattern and the images of the target ROI were captured by a GigE camera (Prosilica GT) with a 2/3″ CCD sensor (Sony ICX625), a maximum resolution of 2448×2050 pixels, a maximum frame rate of 15 fps, and a pixel dimension of 3.45 μm x 3.45 μm. The lens applied to the camera (Rodagon, Edmund Optics) has a focal length of 80 mm with a maximum f-number equal to f/4.0. Image acquisition was performed by a commercial software (Vic-Snap, Correlated Solutions) interfaced with the CCD camera by means of a digital/analog acquisition board (DAQ-STD-8D, National Instruments). The set-up allows to manage different types of synchronization signals and up to two digital cameras simultaneously. A voltage proportional to the displacement of the cross-head of the universal testing machine was used herein to acquire an image every 0.5 mm. A PC workstation with VIC-2D software package (Correlation Solution Inc., version 2009.2.0) was used to store and process the speckle images from which the displacement field was resolved. Fracture tests were carried out using similar experimental set-up. For each sample configuration, three tests were carried out to ensure robustness and significance of the obtained results.

3. Results and discussion

3.1. Baseline samples

The baseline properties of bulk tensile and DCB samples were firstly established. A typical stress-strain plot determined from tensile tests carried out on dogbone samples is reported in Fig. 2(a). The results indicated a non-linear

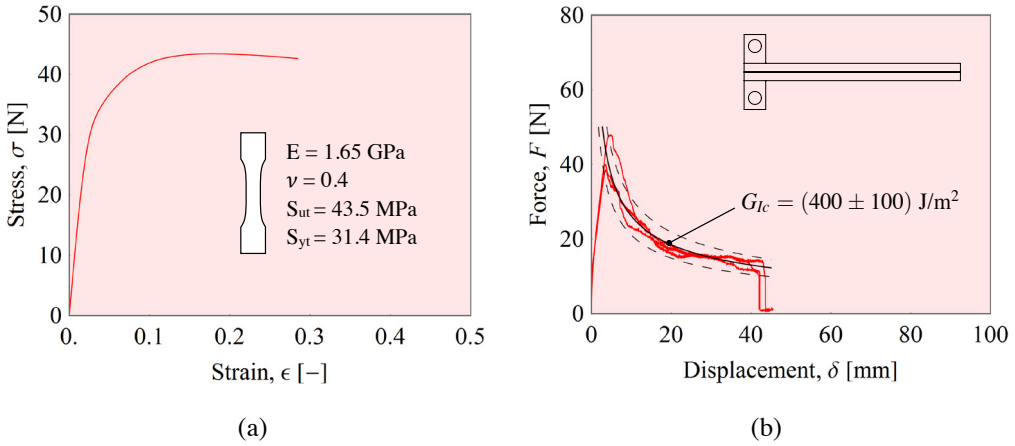

Fig. 2: (a) Stress-strain response recorded on 3D printed dogbone samples. The insert displays the main mechanical properties obtained from testing in conjunction with Digital Image Correlation. (b) Typical load-displacement responses recorded on bulk (*i.e.*, nopatterns) DCB samples. G_{Ic} is the fracture toughness of the joint obtained from the fit with Eq. 1

elastic behavior for the 3D printed material, with Young's modulus E = 1.65 GPa, Poisson's ratio = 0.4 and ultimate strength S_{ut} = 43.5 MPa. The global load-displacement responses obtained in DCB tests with bulk samples are reported in Fig. 2(b). Failure was interfacial and the scatter observed in the softening region was due to crack path deflection from the upper to the lower interface. For comparison, the post peak response predicted using standard Linear Elastic Fracture Mechanics (Anderson, 2005) was used. The plot is obtained using the following equation:

$$\delta = \frac{2\,(b\,G_{Ic})^{3/2}\,\sqrt{EI}}{3F^2}, \tag{1}$$

where δ is the cross-head displacement, b is the sample width, G_{Ic} is the fracture toughness of the joint, E is the Young modulus, I is the moment of inertia and F is the applied peel load. Previous Eq. 1 can be effectively used to identify the toughness of the joints by knowing sample geometry and using the experimentally recorded load-displacement point

data. In particular, G_{Ic} was finely tuned until a good match between experiments and simulations was achieved. An average toughness equal to ≈400 J/m^2 was determined. It is worth noting that the present value is somewhat different from that obtained by the authors in previous works, where the fracture toughness was determined considering samples with metal substrates and was equal to 2700 J/m^2, see Alfano et al. (2011) and Chiodo et al. (2015). However, the difference can be addressed to the peculiar mechanism of failure observed in the experiments, *i.e.* whereas in previous works failure was cohesive within the adhesive layer, herein interfacial failure was observed in all tests.

3.2. Samples with subsurface patterns

The data obtained with bulk samples were employed as baseline results for subsequent comparative analyses with bio-inspired interfaces. The results are reported in Figs. 3(a) and (b). The global responses feature fluctuations in the applied load and it is also apparent that the magnitude is much higher for the channels with square cross-section. The shift of the global response toward higher loads entails an increase in the total work needed to sever the samples. It is interesting to note that the increased energy dissipated in the process came with no additional surface preparation with respect to that employed in the bulk samples discussed earlier.

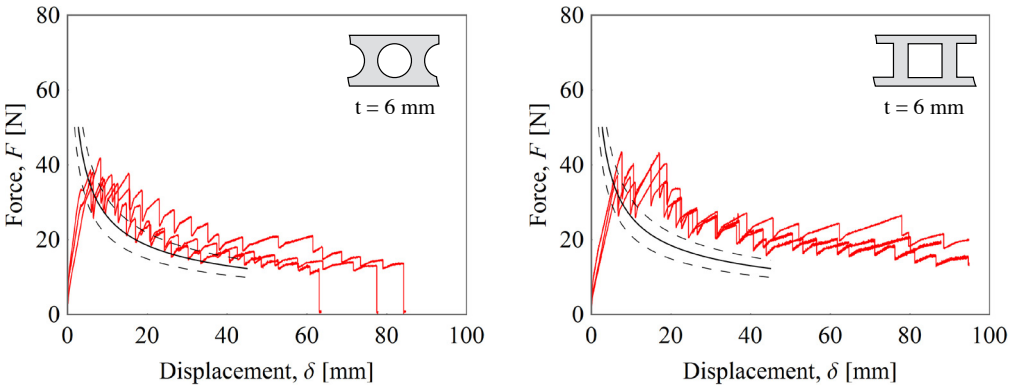

Fig. 3: Global load-displacement responses obtained in DCB tests. (a) Circular channels. (b) Square channels. The continuous black line represents the average of the experimental responses, while the dashed lines represent the overall range of experimental measurements on bulk samples.

3.3. High resolution imaging

The failure mechanism was further investigated through the acquisition of high-resolution images in a region of interest around the advancing crack front. In particular, Fig. 4(a) displays a schematic depiction of the approximate locations on the load-displacement response where the images were taken; the points are lying around a typical load drop recorded in the experiments. The corresponding snapshots allow to conclude that the peak load is achieved when the crack front is approaching the pillars lying between two consecutive channels. In this configuration most of the supplied energy is transferred to the crack tip and it is suddenly released when the crack propagates in unstable fashion to the next pillar. The total work of fracture (WOS) needed to sever the samples was determined as the area below the load-displacement responses. The WOS embeds the fracture energy associated to interfacial failure and the non-recoverable elastic energy suddenly released by the DCB arms when the crack growths in unstable fashion. Moreover, a plastic energy contribution is also included since a small residual deformation of the beams was observed after testing. However, this is deemed negligible with respect to previous contributions. The results are reported in Fig. 4(b) and indicated that the dissipated energy strongly depends on the geometry of the subsurface channels. In particular, channels with a square cross-section provided a significant increase of the WOS, *i.e.* ≈150%.

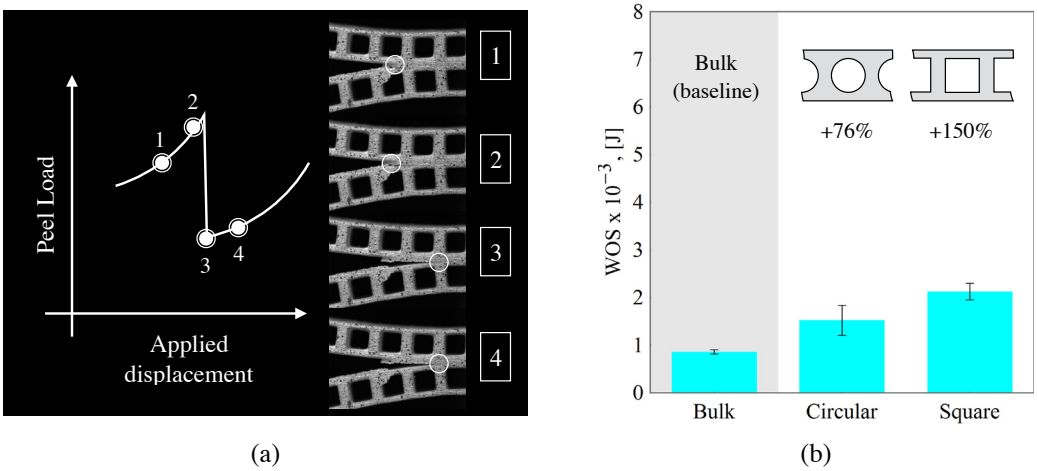

Fig. 4: (a) Snapshots of the fracture process and corresponding locations on schematic load-displacement response. (b) Total work of separation needed to sever the DCB samples.

4. Conclusions

The results of DCB fracture tests have shown that bio-inspired subsurface channels induce a significant increase in the total dissipated energy with respect to bulk samples, *i.e.* no channels. High resolution imaging of the fracture process zone indicated that the observed fluctuations in the global response are related to the sequential storage and sudden release of elastic energy. Crack trapping effectively delayed the crack propagation process and its intensity depended on the subsurface architecture (*i.e.* channel shape). Indeed, it is the spatial modulation of the stiffness around the interfacial region that affects the available driving force for crack growth. This study further confirms that additive manufacturing represents a powerful platform for experimental study of bio-inspired materials. Future developments will focus on the analysis of alternative channel geometries and/or joining techniques.

Acknowledgements

This work was carried out in part in the MaTeRiA Laboratory at University of Calabria.

References

Afferrante, L., Carbone, G., 2011. Biomimetic surfaces with controlled direction-dependent adhesion. Journal of the Royal Society, 9, 3359-3365.

Afferrante, L., Grimaldi, G., Demelio, G., Carbone, G., 2015. Direction-dependent adhesion of micro-walls based biomimetic adhesives. International Journal of Adhesion and Adhesives, 61, 93-98.

Alfano, M., Furgiuele, F., Pagnotta, Paulino, G.H., 2011. Analysis of fracture in aluminum joints bonded with a bi-component epoxy adhesive, Journal of Testing and Evaluation, 39(2).

Anderson, T.L., 2005. Fracture Mechanics. Fundamentals and Applications, ed. CRC-Taylor and Francis.

Beese, A.M., An, Z., Sarkar, S., Shiva, S., Nathamgari, P., Espinosa, H.D., Nguyen, S.T., 2014. Defect-tolerant nanocomposites through bio-inspired stiffness modulation, Advanced Functional Materials, 24, 2883-2891.

Chiodo, G., Alfano, M., Pini, S., Pirondi, A., Furgiuele, F., Groppetti, A., 2015. On the effect of pulsed laser ablation on shear strength and mode I fracture toughness of Al/epoxy adhesive joints. Journal of Adhesion Science and Technology, 29(17), 1820-1830.

Glassmaker, N., Jagota, A., Hui, C.-Y., Noderer, W.L., Chaudhury, M.K. 2007. Biologically inspired crack trapping for enhanced adhesion, Proceedings of the National Academy of Sciences, 104(26), 10786-10791.

Hui, C.-Y., Long, R., Wahl, K.J., Everett, R.K. (2011). Barnacles resist removal by crack trapping. Journal of the Royal Society Interface, 8 (59), pp. 868-879.

Jagota, A., Hui, C.-Y., 2011. Adhesion, friction, and compliance of bio-mimetic and bio-inspired structured interfaces. Materials Science and Engineering R, 72, 253-292.

Libonati, F., Gu, G.X., Qin, Z., Vergani, L., Buehler, M.J. 2016. Bone-inspired materials by design: toughness amplification observed using 3D printing and testing, Advanced Engineering Materials, 18(8), 1354-1363.

Lin, E., Li, Y., Weaver, J.C., Ortiz, C., Boyce, M.C., 2014. Tunability and enhancement of mechanical behaviour with additively manufactured bio-inspired hierarchical suture interfaces. Journal of Materials Research, 29(17), 1867-1875.

Majumder, A., Sharma, A., Ghatak, A., 2010. Bio-inspired adhesion and adhesives: controlling adhesion by micro-nano structuring of soft substrates in S. Chakraborty (ed.), Microfluidics and Microfabrication, DOI 10.1007/978-1-4419-1543-6-7, Springer Science.

Standard Test Method for Tensile Properties of Plastics, ASTM D638-14(2014).